Inorganic Chemistry

pubs.acs.org/IC

Article

Position-Induced Controllable Growth of Vertically Oriented Graphene Using Plasma-Enhanced Chemical Vapor Deposition

Yifei Ma, Jiemin Han, Dewu Yue,* Zhaomin Tong, Mei Wang,* Liantuan Xiao, Suotang Jia, and Xuyuan Chen

Cite This: *Inorg. Chem.* 2023, 62, 13505−13511

Read Online

ACCESS | Metrics & More | Article Recommendations | Supporting Information

ABSTRACT: Because the morphology of vertically oriented graphene (VG) synthesized by the plasma-enhanced chemical vapor deposition process determines the application performance of VG, morphology control is always an important part of the research. A concise correspondence between plasma and the morphology of VG is the key to investigating the morphology control of VG, which is still under research. In this study, a simple but effective parameter, position, is used to grow VG, by which the continuous morphology evolution of VG is realized. As a result, the morphology of VGs varies from a porous structure to a "wall-like" structure, thus leading to a continuous change in its hydrophobicity and thermal emissivity. An ultrahigh emissivity of 0.999 with superhydrophobicity is obtained among these VGs, showing great potential in the area of the black body and infrared thermometer. Finally, the states of active particles in plasma depending on the positions are diagnosed to investigate their relations with the morphology of VGs.

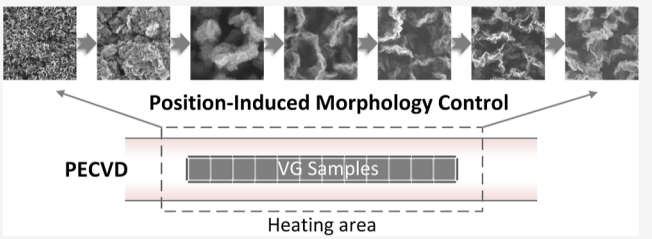

1. INTRODUCTION

In the last 18 years, no other material has stood out as much as graphene among remarkable carbon-based materials.[1] Graphene has demonstrated excellent performance in many applications, such as optoelectronics[2] and sensors,[3,4] raising the prospect of future innovation in the fields of flexible, transparent, and ultralight nanodevices. Moreover, its derivatives, such as graphene quantum dots,[5] graphene mesh,[6] and doped graphene,[7] offer improved efficiency and extended capacities in several applications, mostly owing to their size, structure, or doping effects. Among such materials, vertically oriented graphene (VG) synthesized using plasma-enhanced chemical vapor deposition (PECVD) has not only inherited the intrinsic properties of graphene but also reaped the benefits from a spatial structure that facilitates a large active surface area, exposed sharp edges, and a non-stacking structure.[8] Therefore, VG performs excellently in various applications such as supercapacitors,[9] catalysts,[10] solar cells,[11] and ultrahigh light absorbers.[12]

As a three-dimensional material, the spatial structure plays an important role in the properties of VG. For example, Miller et al. developed a high-response capacitor based on VG with a "wall-like" structure that can serve as an AC filter;[13] moreover, our previous research demonstrated VG with a "tree-like" structure that exhibits excellent flexibility and durability as an electrode for wearable supercapacitors.[9,14] Therefore, massive efforts have been made to control the morphology of VG, both theoretically and experimentally.[15,16] The most common way to control the morphology and properties of VG is to control the routine synthesis conditions, such as growth temperature, plasma source power, growth time, precursors, and substrates.[11,16−21] However, they can just slightly adjust the basic morphology of VG, like height, density of graphene flakes, size of VG flakes, and so forth. Then, some research induces extra control methods to break the limitation of routine synthesis. For example, electric fields[22,23] (or magnetic fields[24]) are added in PECVD by plate electrodes (or solenoids) to influence the growth process of VG, by which the growth location and structure of VG flakes are adjusted.

Up to now, three typical morphologies of VG have been reported, the "wall-like" structure,[8] the "tree-like" structure,[9] and the porous structure.[21] However, the morphology transformation from one morphology to another has not been achieved by changing one of the aforementioned factors. It requires changing both the plasma source power and temperature,[20] increasing the complexity of the control process and the study of the growth mechanism.

Theoretically, the morphology and the properties of VG are determined by the growth process, which is directly associated with states of plasma during the growth. The regulation of the morphology of VG depending on the plasma state could

Received: June 9, 2023
Published: August 10, 2023

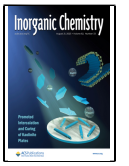

provide insight into the growth mechanism of VG and the key to controlling the morphology of VG. However, the plasma deposition process is quite complex and involves physical and chemical processes, setting a great obstacle to the study of the growth mechanism. Therefore, a simple and direct correspondence between the plasma state and the morphology of VG is required.

In this study, the position-induced plasma state and morphological evolution of VG have been investigated in a tube-type PECVD instrument. Unlike previously reported research, the growth position will impact the morphology and properties of VG, which change considerably from a porous structure to "tree-like" graphene and then to "wall-like" graphene, covering almost all existing morphologies of VG. Furthermore, by changing only the position parameter, a continuous change in morphology rather than a discrete change is obtained, making the deposition process considerably simpler. Benefiting from the morphology, VG with superhydrophobicity and ultrahigh emissivity (0.999) is obtained, which can be used as a standard reference to measure the temperature and emissivity of unknown objects using an infrared thermometer. We strongly believe that this study will provide a new approach to investigating the VG growth mechanism in depth.

2. EXPERIMENTAL SECTION

2.1. Preparation of VG. In this study, a 5 × 40 cm^2 quartz plate was used in the heating area of the PECVD instrument as a substrate holder (Figure 1). The heating area was composed of 4 independent

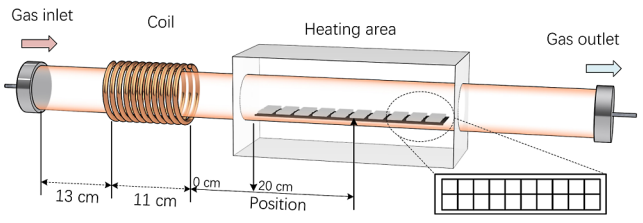

Figure 1. Schematic illustration of the tube-type PECVD instrument.

heaters with a temperature controller for each, and each heater controlled a quarter of the heating area. Then, the temperature could be precisely controlled and the temperature variation could be well suppressed. After cleaning, 2 × 2 cm^2 quartz plates were densely placed next to each other on that holder. To indicate the position, the right end of the plasma antenna was set as the zero point, based on which the relative position of the VG sample was labeled. Afterward, the PECVD chamber was cleaned using hydrogen gas at a flow rate of 8 sccm and a temperature of 900 °C for 5 min to remove the surface oxide on the quartz substrate. The temperature inside the chamber was measured and controlled using a temperature probe and heater, respectively. Subsequently, plasma was generated for 3 min using a radiofrequency source power of 200 W to further remove contaminants on the substrate. Graphene was then grown for 60 min at a temperature of 900 °C and a plasma source power of 500 W by introducing C_2H_2 and H_2 at flow rates of 6 and 2 sccm, respectively.

2.2. Characterizations of VG. The surface and cross-sectional morphologies of the VG samples on quartz substrates were examined via field emission scanning electron microscopy (HITECH, SU8000). The sheet resistance was measured using the four-point probe method (Ningbo Argal Instrument Co., Ltd., FT-341) by selecting 10 random points on the surface of each sample. The detector equipped with linearly arranged four probes was perpendicularly contacted with the surface of the sample at room temperature without additional treatment. The static contact angles were measured by dropping 5 μL of water droplets on the VG surfaces through a syringe device and analyzed using a digital goniometer (KRÜSS, DSA25B). An infrared imager (Flir, E85) and related software (Flir, ResearchIR) were used to measure the temperature and analyze emissivity.

2.3. Plasma Diagnostic. The optical emission spectrum from the plasma was monitored with an optical fiber-coupled high-speed spectrometer (Ideaoptics, PG2000). The electron temperature and ion density of the plasma were measured by a Langmuir probe (Impedans, ALP 150) with a double probe.

3. RESULTS AND DISCUSSION

Along with the flow direction of the source plasma stream, the most immediate changes in VG embody varying morphologies. Figure 2a shows the morphological evolution of the VG samples from the top at the available deposition areas. Herein, we set the right end of the plasma antenna as the starting point (0 cm) to mark the relative position of the VG sample (Figure 1). The available growth position is limited by the antenna shield and the insulator of the heater; thus, it starts from 20 cm and ends at 58 cm according to the starting point. As shown in Figure 2a, the entire evolution process could be approximately divided into three stages. In the initial stage, the growth position ranging from 20 to 30 cm, dense structures with small flakes were observed. These films exhibit a morphology different from that of a typical VG and were considered porous films.[21] Subsequently, the porous structure gradually separated and generated trenches in the downstream direction. In the second stage, the growth position ranging from 30 to 34 cm, the previous porous structure developed into thick but agminated flakes, exhibiting a typical "tree-like" graphene structure.[9,14] In the last stage, the growth position ranging from 36 cm to the end, the VG flakes continuously became thinner and twisted, showing the morphology of a "wall-like" graphene structure.

In accordance with the top-view morphology, the cross-sectional views of the VG samples (Figure S1) revealed the increased gaps between the flakes and decreased thickness of the flakes when increasing the distance away from the zero point. As shown in Figure 2b, the height of the VG samples (measured from Figure S1) continuously decreased with an acceptable fluctuation. The reduced height of the VG samples reduced the connection between graphene flakes. Therefore, the sheet resistance continuously increased with decreasing height, as depicted in Figure 2c.

Some of the properties, for example, wettability, playing an important role in practical applications, are closely related to the surface microstructure of VG. Therefore, the contact angle of the VG samples was investigated (Figure 3) and found to vary with their surface morphology. The VG samples located from 20 to 34 cm had relatively larger densities of graphene flakes, resulting in higher contact angles. Their average contact angle reached 150.0°, with the highest being 153.6° for the VG sample at 30 cm. The other VG samples exhibited relatively lower contact angles with an average value of 139.1°, with the lowest being 137.3° for the VG sample at 40 cm.

The contact angle is related to the structure of the surface. As previously reported by Ghosh[25] and Bo,[26] the observed wetting properties of VG vary with densities of vertical fakes, which can be described using the Cassie theory. The apparent contact angle (θ_r) related to the real contact angle (θ_e) in the ideal Cassie mode can be calculated as follows

$$\cos\theta_r = \varphi\cos\theta_e + \varphi - 1 \quad (1)$$

https://doi.org/10.1021/acs.inorgchem.3c01893
Inorg. Chem. 2023, 62, 13505−13511

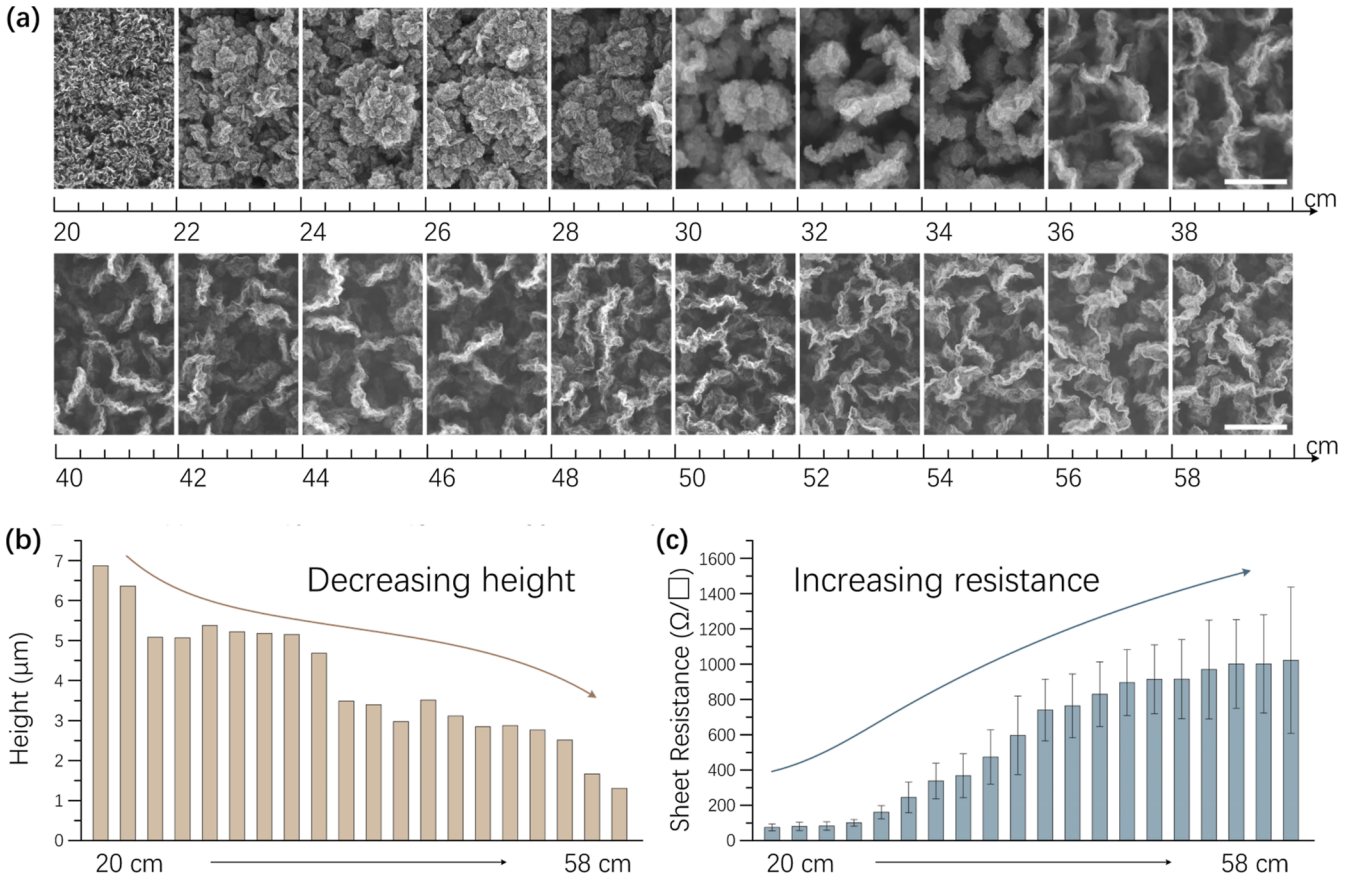

Figure 2. (a) Top SEM images of the structure evolution of VG samples grown at different positions. The scale bar is 1 μm. (b,c) Height and sheet resistance of VG samples grown at different positions.

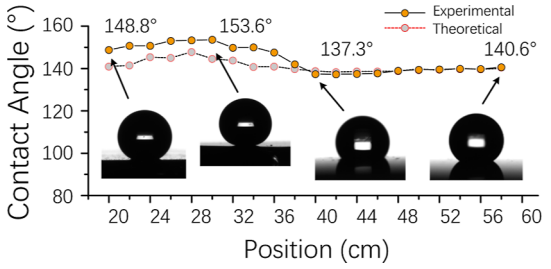

Figure 3. Contact angle changes depending on the growth position.

where φ denotes the area ratio of the projected area to the surface area of the material without any features. Here, the real contact angle (θ_e) is considered to be the same as that of graphite (95°).[25] Furthermore, the projected area of the VG samples was extracted from Figure S2 and analyzed using the aforementioned equation. As plotted in Figure 3, the calculated contact angles exhibited a trend similar to that of the experimental contact angles.

Besides the contact angle, thermal emissivity is strongly influenced by the surface condition of VG. Infrared thermometers are based on the most basic theory that all objects emit thermal radiation at >0 K. However, for any particular object, the amount of thermal radiation emitted from a surface depends not only on the material but also on the nature of the surface. The emissivities of the VG samples range were measured and calculated (the method is described in the Supporting Information). As shown in Figure 4a, the emissivity change of the VG samples depending on growth position or surface morphology was tested at 40 °C. The minimum

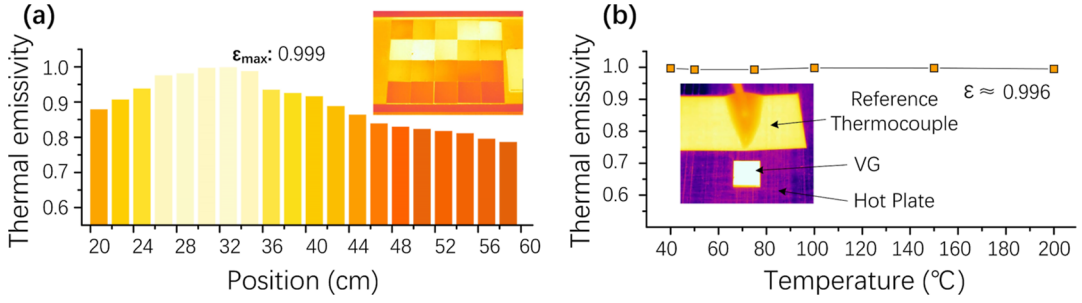

Figure 4. (a) Thermal emissivity variation of VG samples depending on the position at 40 °C. (b) Emissivity stability of VG at 32 cm with different temperatures.

https://doi.org/10.1021/acs.inorgchem.3c01893
Inorg. Chem. 2023, 62, 13505−13511

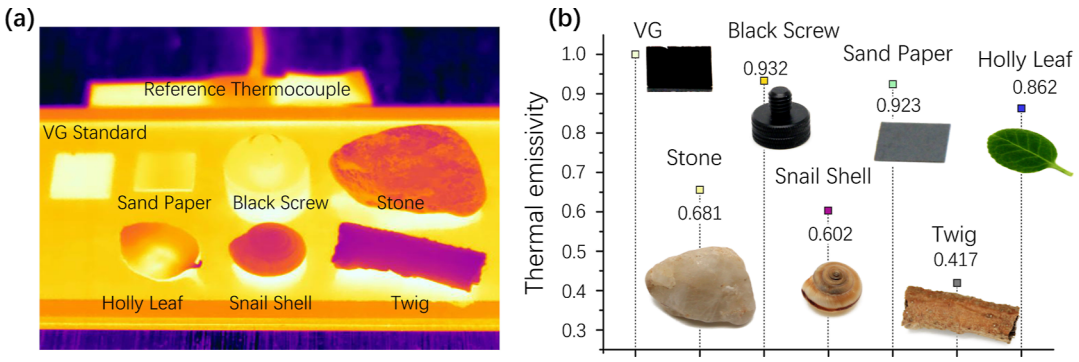

Figure 5. Image from infrared thermometry (a) and emissivity of diverse objects (b).

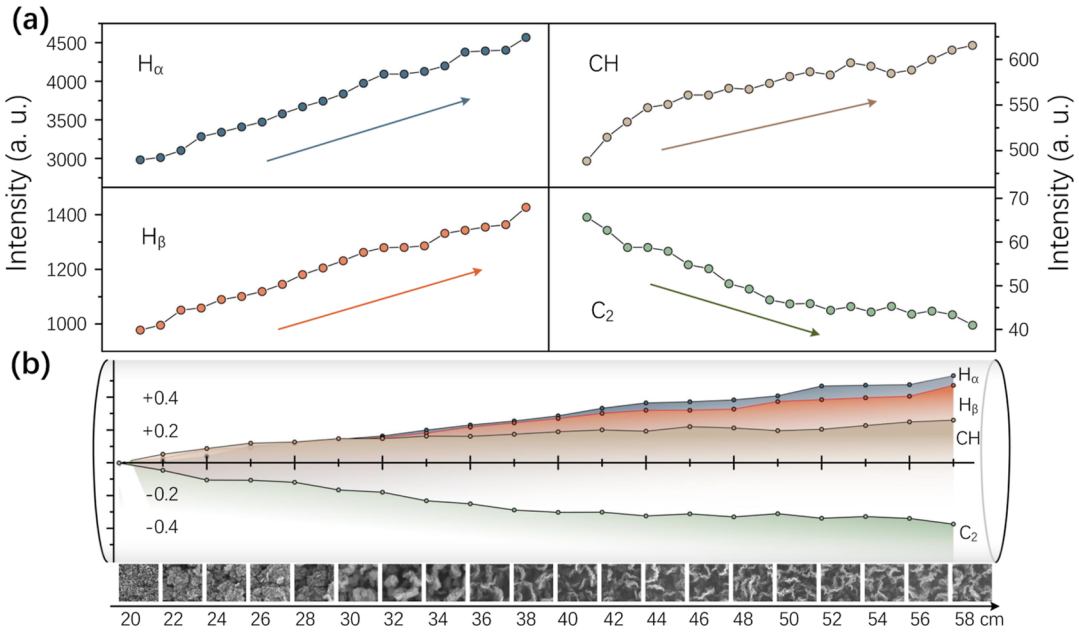

Figure 6. Radical densities (H_α at 656.3 nm, H_β at 486.1 nm, CH at 431.4 nm, and C_2 at 516.5 nm[30]) (a) and their increment (b) depending on the position.

emissivity of 0.787 was obtained at 58 cm, whereas the maximum emissivity of 0.999 was obtained at 32 cm. Furthermore, the emissivity of VG at 32 cm was considerably stable, with an emissivity of ~0.996 at temperatures ranging from 40 to 200 °C (Figure 4b).

The high emissivity of VG could be described from another perspective, that is, light absorption. Kirchhoff's law of thermal radiation states that any object radiating and absorbing is in thermodynamic equilibrium at any given temperature, that is, $\varepsilon_{emission} = \alpha_{absorption}$. In other words, the strong radiation of the VG samples indicates strong absorption and vice versa. Typical VG has unique vertically oriented flakes and gaps in between, forming a microwell that traps incident light (Figure S3), as reported in previous research;[12] therefore, the proper size of gaps and flakes will endow VG with strong absorption of light and, in turn, strong emission.

It is worth noting that the highest contact angle and thermal emissivity are both achieved by VG around the position of 31 cm, which is typically named as the "tree-like" structure. In this structure, "trees" are composed of randomly stacked graphene nano-sheets.[9] As confirmed by Figures 2 and S1, the "tree-like" structure is much sparse with larger inter-tree spacing than the porous and "wall-like" structures. According to the aforementioned Cassie theory, this sparse "tree-like" structure provides a low projected area ratio as shown in Figure S2 and Table S1, thus leading to a high contact angle. In addition, the large inter-tree spacing and low projected area ratio of the "tree-like" structure can reduce the surface reflection while trapping the incident light in the gaps between "trees",[12] hence showing strong light absorption and strong emission as well.

VG has good thermal conductivity,[27] which will quickly reach temperature equilibrium with the environment, making VG a facile standard black body useful in infrared thermometry. A complex reference experiment is required to detect the temperature or emissivity of an unknown object using an infrared thermometer.[28,29] However, by attaching VG with high emissivity to a target object as a reference, both the temperature and emissivity can be determined facilely. To demonstrate the usage of VG, a stone, a piece of sandpaper, a leaf, a snail shell, a screw, a twig, and VG (at 32 cm) were placed on a hot plate under monitoring with an infrared thermometer (Figure 5a). Because VG exhibits a stable emissivity of 0.996 at temperatures ranging from 40 to 200 °C, by setting the emissivity of VG, the temperature of the plate, which was 40.3 °C, could be easily read out from the infrared thermometer. The same temperature was also

https://doi.org/10.1021/acs.inorgchem.3c01893
Inorg. Chem. 2023, 62, 13505−13511

detected from the reference thermocouple. The parts of the samples in contact with the plate will have the same temperature as the plate; accordingly, their emissivity can be easily obtained via infrared thermometry (Figure 5b).

The active particles (radicals, ions, etc.) in plasma play an most important role in VG growth. However, these particles are dynamically connected through ionization and collision, whose balance is easily influenced by growth conditions, setting considerable obstacles to controlling and clarifying the roles of particles during VG growth. This study has proposed a steady growth process without any change in growth conditions so that the reactions of active particles also remain in a dynamic balance. The condition of active particles only varies with growth position, as does the VG morphology. Thus, the morphological change of VG can be associated with only the condition of active particles.

The noncontact plasma diagnostic approach, that is, optical emission spectroscopy, was performed to investigate the change in radical intensities. As reported in other research, H, CH, and C_2 radicals play an important role in the growth of graphene:[15,30] the H radical has a strong etching effect; the CH radical serves as the terminator that prevents graphene growth, whereas the C_2 radical promotes VG growth. In this research, as depicted in Figure 6a, the intensities of H radicals (H_α at 656.3 nm and H_β at 486.1 nm) and CH radicals (431.4 nm) increase with position, whereas the intensity of C_2 radicals (516.5 nm) decreases.[30] Compared with the radical intensities at the initial growth point (20 cm), the intensities of H_α, H_β, and CH radicals at 58 cm increased by 53, 47, and 25%, respectively, whereas that of C_2 radicals decreased by 38% (Figure 6b). According to previous studies,[15,31,32] these changes in radicals indicate the increased etching and terminating force with a decreased deposition force; thus, it is not difficult to predict that the VG samples along the downstream direction will become sparse and short, which could be confirmed by the morphological change of the VG samples from the SEM images shown in Figures 2 and S1.

Owing to the sheath effect in plasma, ions will be accelerated to impact the substrate and contribute to VG growth. Herein, a Langmuir probe was used to detect ion profiles depending on the position. As depicted in Figure 7a, the electron temperature decreased with increasing position, indicating a fading activity of plasma along the downstream direction. Furthermore, the floating sheath potential can be obtained using the electron temperature through the following equation[33]

$$V_f = \frac{kT_e}{2e}\ln\left(\frac{2\pi m_e}{M}\right) \quad (2)$$

where V_f denotes the floating sheath potential in the plasma, k denotes the Boltzmann constant, T_e denotes the electron temperature, e denotes the elementary charge, m_e denotes the electron mass, and M denotes the ion mass. According to the aforementioned equation, the floating sheath potential, V_f, is proportional to the electron temperature, T_e. Therefore, the decreasing electron temperature with increasing growth position indicates a decrease in the floating sheath potential. The sheath potential will accelerate the ions to impact the substrate and participate in the growth process. As the sheath potential decreases, the kinetic energy of the ions distributed by the sheath decreases,[34] then decreasing the reaction rate of ions on the substrate. Additionally, Figure 7b illustrates that the density of ions decreases depending on the position. In plasma, because ions and neutral particles (radicals, atoms, and molecules) can convert to each other by collision,[35] it is reasonable that ion density decreases while the radical intensity increases (Figure 6). In addition, the decreased ion density means that the number of ions is decreased. Hence, irrespective of the role (deposition or etching) that ions played in VG growth, the reaction rate of ions is decreased. Overall, both the activity and density of ions decreased along with the plasma downstream, leading to a decreased reaction rate of ions on the substrate.

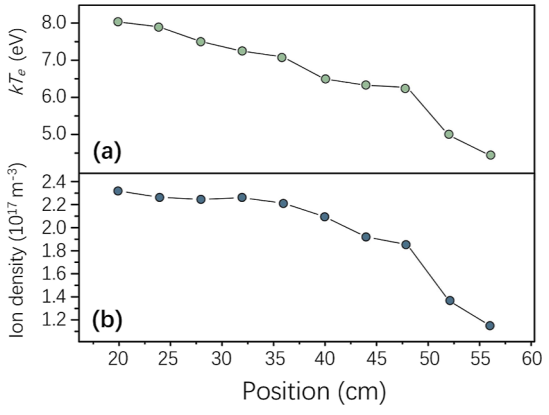

Figure 7. Electron temperature (a) and ion density (b) depending on the position.

4. CONCLUSIONS

In this study, the position-induced morphological evolution of VG in a tube-type PECVD instrument and VG properties depending on VG morphology were investigated. The continuously changing morphology of VG demonstrates continuous property tuning, resulting in contact angles ranging from 137.3 to 153.6° and thermal emissivity ranging from 0.787 to 0.999. Such a high thermal emissivity has made graphene capable of serving as a standard black body. The morphology change can be attributed to the gradient of the plasma stream and is related to the active particles in the plasma. A high intensity of C_2 with low intensity of CH and H results in a high density of VG flakes and vice versa. A low electron temperature leads to a low sheath potential, thus decreasing the impact energy of the ions. Customized VG morphology and properties can be realized by changing the position or by controlling the intensity of the main radicals. However, the state of plasma is hard to be controlled precisely owing to the complexity of the plasma process; therefore, the control of position is recommended. We strongly believe that this study will promote the controllable synthesis of VG and the use of VG with optimized properties.

■ ASSOCIATED CONTENT

Supporting Information

The Supporting Information is available free of charge at https://pubs.acs.org/doi/10.1021/acs.inorgchem.3c01893.

Cross-sectional and top SEM images of VGs, extracted projected area images of VGs, ratios of the projected area of VGs, and method for emissivity measurement (PDF)

https://doi.org/10.1021/acs.inorgchem.3c01893
Inorg. Chem. 2023, 62, 13505−13511

AUTHOR INFORMATION

Corresponding Authors

Dewu Yue − *Information Technology Research Institute, Shenzhen Institute of Information Technology, Shenzhen 518172, China*; Email: yuedewu@sziit.edu.cn

Mei Wang − *State Key Laboratory of Quantum Optics and Quantum Optics Devices, Institute of Laser Spectroscopy, Collaborative Innovation Center of Extreme Optics, Shanxi University, Taiyuan 030006, China*; orcid.org/0000-0003-4127-4983; Email: wangmei@sxu.edu.cn

Authors

Yifei Ma − *State Key Laboratory of Quantum Optics and Quantum Optics Devices, Institute of Laser Spectroscopy, Collaborative Innovation Center of Extreme Optics, Shanxi University, Taiyuan 030006, China*

Jiemin Han − *State Key Laboratory of Quantum Optics and Quantum Optics Devices, Institute of Laser Spectroscopy, Collaborative Innovation Center of Extreme Optics, Shanxi University, Taiyuan 030006, China*

Zhaomin Tong − *State Key Laboratory of Quantum Optics and Quantum Optics Devices, Institute of Laser Spectroscopy, Collaborative Innovation Center of Extreme Optics, Shanxi University, Taiyuan 030006, China*

Liantuan Xiao − *State Key Laboratory of Quantum Optics and Quantum Optics Devices, Institute of Laser Spectroscopy, Collaborative Innovation Center of Extreme Optics, Shanxi University, Taiyuan 030006, China*

Suotang Jia − *State Key Laboratory of Quantum Optics and Quantum Optics Devices, Institute of Laser Spectroscopy, Collaborative Innovation Center of Extreme Optics, Shanxi University, Taiyuan 030006, China*

Xuyuan Chen − *State Key Laboratory of Quantum Optics and Quantum Optics Devices, Institute of Laser Spectroscopy, Collaborative Innovation Center of Extreme Optics, Shanxi University, Taiyuan 030006, China; Faculty of Technology, Natural Sciences and Maritime Sciences, Department of Microsystems, University of Southeast Norway, Borre N3184, Norway*

Complete contact information is available at: https://pubs.acs.org/10.1021/acs.inorgchem.3c01893

Author Contributions

Y.M. and J.H. contributed equally to this work. Y.M. participated in the data curation, formal analysis, funding acquisition, writing—original draft, and writing—review and editing. J.H. performed the data curation and writing—original draft. D.Y. executed the supervision, funding acquisition, and writing—review and editing. Z.T. carried out the methodology and supervision. M.W. executed the conceptualization, supervision, funding acquisition, and writing—review and editing. L.X. conducted the supervision, funding acquisition, and writing—review and editing. S.J. implemented the supervision, funding acquisition, and writing—review and editing. X.C. accomplished the supervision and writing—review and editing.

Notes

The authors declare no competing financial interest.

ACKNOWLEDGMENTS

This research was supported by the National Key R&D Program of China (grant no. 2022YFA1404001), the National Natural Science Foundation of China (grants nos 51902190 and 12104319), research project supported by the Shanxi Scholarship Council of China (2021-004 and 2022-013), the 111 Project (grant no. D18001), the Changjiang Scholars and Innovative Research Team at the University of Ministry of Education of China (grant no. IRT_17R70), and the Fund for Shanxi "1331 Project" Key Subjects, the Double High-levels Plan (11400-2023-020201-04061).

REFERENCES

(1) The graphene times, *Nat. Nanotechnol.*, *14* (**2019**) 903. DOI: 10.1038/s41565-019-0561-4

(2) Bonaccorso, F.; Sun, Z.; Hasan, T.; Ferrari, A. C. Graphene photonics and optoelectronics. *Nat. Photonics* **2010**, *4*, 611−622.

(3) Kaidarova, A.; Khan, M. A.; Marengo, M.; Swanepoel, L.; Przybysz, A.; Muller, C.; Fahlman, A.; Buttner, U.; Geraldi, N. R.; Wilson, R. P.; Duarte, C. M.; Kosel, J. Wearable multifunctional printed graphene sensors. *npj Flexible Electron.* **2019**, *3*, 15.

(4) Hwang, M. T.; Heiranian, M.; Kim, Y.; You, S.; Leem, J.; Taqieddin, A.; Faramarzi, V.; Jing, Y.; Park, I.; van der Zande, A. M.; Nam, S.; Aluru, N. R.; Bashir, R. Ultrasensitive detection of nucleic acids using deformed graphene channel field effect biosensors. *Nat. Commun.* **2020**, *11*, 1543.

(5) Chung, S.; Revia, R. A.; Zhang, M. Graphene quantum dots and their applications in bioimaging, biosensing, and therapy. *Adv. Mater.* **2021**, *33*, 1904362.

(6) Cho, E. H.; Kim, M. J.; Sohn, H.; Shin, W. H.; Won, J. Y.; Kim, Y.; Kwak, C.; Lee, C. S.; Woo, Y. S. A graphene mesh as a hybrid electrode for foldable devices. *Nanoscale* **2018**, *10*, 628−638.

(7) Lin, L.; Li, J.; Yuan, Q.; Li, Q.; Zhang, J.; Sun, L.; Rui, D.; Chen, Z.; Jia, K.; Wang, M.; Zhang, Y.; Rummeli, M. H.; Kang, N.; Xu, H. Q.; Ding, F.; Peng, H.; Liu, Z. Nitrogen cluster doping for high-mobility/conductivity graphene films with millimeter-sized domains. *Sci. Adv.* **2019**, *5*, No. eaaw8337.

(8) Li, J.; Liu, Z.; Guo, Q.; Yang, S.; Xu, A.; Wang, Z.; Wang, G.; Wang, Y.; Chen, D.; Ding, G. Controllable growth of vertically oriented graphene for high sensitivity gas detection. *J. Mater. Chem. C* **2019**, *7*, 5995−6003.

(9) Ma, Y.; Wang, M.; Kim, N.; Suhr, J.; Chae, H. A flexible supercapacitor based on vertically oriented 'Graphene Forest' electrodes. *J. Mater. Chem. C* **2015**, *3*, 21875−21881.

(10) Su, D.; Han Seo, D.; Ju, Y.; Han, Z.; Ostrikov, K.; Dou, S.; Ahn, H.-J.; Peng, Z.; Wang, G. Ruthenium nanocrystal decorated vertical graphene nanosheets@Ni foam as highly efficient cathode catalysts for lithium-oxygen batteries. *NPG Asia Mater.* **2016**, *8*, No. e286.

(11) Pan, X.; Zhu, K.; Ren, G.; Islam, N.; Warzywoda, J.; Fan, Z. Electrocatalytic properties of a vertically oriented graphene film and its application as a catalytic counter electrode for dye-sensitized solar cells. *J. Mater. Chem. A* **2014**, *2*, 12746−12753.

(12) Han, J.; Ma, Y.; Wang, M.; Tong, Z.; Suhr, J.; Xiao, L.; Jia, S.; Chen, X. Nano-and micro-engineered vertical graphene/Ni for superior optical absorption. *Appl. Surf. Sci.* **2022**, *606*, 154922.

(13) Miller, J. R.; Outlaw, R. A.; Holloway, B. C. Graphene double-layer capacitor with ac line-filtering performance. *Science* **2010**, *329*, 1637−1639.

(14) Wang, M.; Ma, Y. Nitrogen-doped graphene forests as electrodes for high-performance wearable supercapacitors. *Electrochim. Acta* **2017**, *250*, 320−326.

(15) Baranov, O.; Levchenko, I.; Xu, S.; Lim, J. W. M.; Cvelbar, U.; Bazaka, K. Formation of vertically oriented graphenes: what are the key drivers of growth. *2D Mater.* **2018**, *5*, 044002.

(16) Shuai, X.; Bo, Z.; Kong, J.; Yan, J.; Cen, K. Wettability of vertically-oriented graphenes with different intersheet distances. *RSC Adv.* **2017**, *7*, 2667−2675.

(17) Thomas, R.; Rao, G. M. Synthesis of 3-dimensional porous graphene nanosheets using electron cyclotron resonance plasma enhanced chemical vapour deposition. *RSC Adv.* **2015**, *5*, 84927−84935.

(18) Alancherry, S.; Jacob, M. V.; Prasad, K.; Joseph, J.; Bazaka, O.; Neupane, R.; Varghese, O. K.; Baranov, O.; Xu, S.; Levchenko, I.; Bazaka, K. Tuning and fine morphology control of natural resource-derived vertical graphene. *Carbon* **2020**, *159*, 668−685.
(19) Zhu, S.; Zhang, H.; Wang, J.; Zhao, B.; Wan, D. Research on the defect types transformation induced by growth temperature of vertical graphene nanosheets. *J. Alloys Compd.* **2019**, *781*, 1048−1053.
(20) Xie, S.; Huang, J.; Zhang, Y.; Cai, W.; Zhang, X. Effect of substrate types on the structure of vertical graphene prepared by plasma-enhanced chemical vapor deposition. *Nanomaterials* **2021**, *11*, 1268.
(21) Ma, Y.; Jiang, W.; Han, J.; Tong, Z.; Wang, M.; Suhr, J.; Chen, X.; Xiao, L.; Jia, S.; Chae, H. Experimental investigation on vertically oriented graphene grown in a plasma-enhanced chemical vapor deposition process. *ACS Appl. Mater. Interfaces* **2019**, *11*, 10237−10243.
(22) Shen, C.; Xu, S.; Chen, Z.; Ji, N.; Yang, J.; Zhang, J. Fluorobenzene and water-promoted rapid growth of vertical graphene arrays by electric-field-assisted PECVD. *Small* **2023**, *19*, 2207745.
(23) Yu, K.; Wang, P.; Lu, G.; Chen, K.; Bo, Z.; Chen, J. Patterning vertically oriented graphene sheets for nanodevice applications. *J. Phys. Chem. Lett.* **2011**, *2*, 537−542.
(24) Seo, D. H.; Kumar, S.; Ostrikov, K. Control of morphology and electrical properties of self-organized graphenes in a plasma. *Carbon* **2011**, *49*, 4331−4339.
(25) Ghosh, M.; Anand, V.; Gowravaram, M. R. Wetting characteristics of vertically aligned graphene nanosheets. *Nanotechnology* **2018**, *29*, 385703.
(26) Bo, Z.; Tian, Y.; Han, Z. J.; Wu, S.; Zhang, S.; Yan, J.; Cen, K.; Ostrikov, K. Tuneable fluidics within graphene nanogaps for water purification and energy storage. *Nanoscale Horiz.* **2017**, *2*, 89−98.
(27) Xu, S.; Wang, S.; Chen, Z.; Sun, Y.; Gao, Z.; Zhang, H.; Zhang, J. Electric-field-assisted growth of vertical graphene arrays and the application in thermal interface materials. *Adv. Funct. Mater.* **2020**, *30*, 2003302.
(28) Ficker, T. Virtual emissivities of infrared thermometers. *Infrared Phys. Technol.* **2021**, *114*, 103656.
(29) Davami, K.; Cortes, J.; Hong, N.; Bargatin, I. Vertical graphene sheets as a lightweight light absorber. *Mater. Res. Bull.* **2016**, *74*, 226−233.
(30) Terasawa, T.-o.; Saiki, K. Growth of graphene on Cu by plasma enhanced chemical vapor deposition. *Carbon* **2012**, *50*, 869−874.
(31) Mironovich, K. V.; Itkis, D. M.; Semenenko, D. A.; Dagesian, S. A.; Yashina, L. V.; Kataev, E. Y.; Mankelevich, Y. A.; Suetin, N. V.; Krivchenko, V. A. Tailoring of the carbon nanowall microstructure by sharp variation of plasma radical composition. *Phys. Chem. Chem. Phys.* **2014**, *16*, 25621−25627.
(32) Fu, W.; Zhao, X.; Zheng, W. Growth of vertical graphene materials by an inductively coupled plasma with solid-state carbon sources. *Carbon* **2021**, *173*, 91−96.
(33) Chabert, P. What is the size of a floating sheath? *Plasma Sources Sci. Technol.* **2014**, *23*, 065042.
(34) Liu, J.; Huppert, G. L.; Sawin, H. H. Ion bombardment in rf plasmas. *J. Appl. Phys.* **1990**, *68*, 3916−3934.
(35) Fisher, E. R. On the interplay between plasma ions, radicals and surfaces: who dominates the interaction? *Plasma Sources Sci. Technol.* **2002**, *11*, A105.

https://doi.org/10.1021/acs.inorgchem.3c01893
Inorg. Chem. 2023, 62, 13505−13511